1999

A Mathematical Model for Electroless Copper Deposition on Planar Substrates

M. Ramasubramanian
University of South Carolina - Columbia

Branko N. Popov
University of South Carolina - Columbia, popov@engr.sc.edu

Ralph E. White
University of South Carolina - Columbia, white@cec.sc.edu

K. S. Chen

Publication Info

Journal of the Electrochemical Society, 1999, pages 111-116.

Publisher's link: http://dx.doi.org/10.1149/1.1391572
DOI: 10.1149/1.1391572

Journal of The Electrochemical Society, **146** (1) 111-116 (1999)
S0013-4651(98)02-031-X CCC: $7.00 © The Electrochemical Society, Inc.

A Mathematical Model for Electroless Copper Deposition on Planar Substrates

M. Ramasubramanian,[a,*] B. N. Popov,[a,] R. E. White,[a,**] and K. S. Chen[b,**]**

[a]*Center for Electrochemical Engineering, Department of Chemical Engineering, University of South Carolina, Columbia, South Carolina 29208, USA*
[b]*Sandia National Laboratories, Engineering Sciences Center, Albuquerque, New Mexico 87185-0826, USA*

A mathematical model for the electroless deposition of copper on a planar electrode is presented and used to make time-dependent predictions on the various quantities in the system. The model takes into account mass transport by diffusion and migration, Butler-Volmer kinetics at the electrode surface, and mixed potential theory. A finite difference approach is used to solve the equations, and the resultant model is used to predict the concentration profiles, potential response, and plating rate as a function of time and concentration of various reactive components.

Manuscript submitted February 9, 1998; revised manuscript received May 22, 1998.

Mixed potential theory has been used to explain electroless deposition processes, initially by Paunovic[1] and subsequently by Donahue.[2] The electroless plating process has been ascribed to occur due to a combination of the partial electrode oxidation and reduction processes, the rates of which are equal and opposing in nature at all times. Both the oxidation and reduction reactions occur at the same electrode during electroless plating, and the driving forces for these reactions arise from the potential difference that exists between the metal-solution interface and the equilibrium electrode potential for these (cathodic and anodic) half-reactions. In a typical electroless copper deposition system, the copper reduction and formaldehyde oxidation are the cathodic and anodic reactions, respectively. Electroless deposition will continue to occur as long as a positive driving force exists for both of these reactions, and the rate of reaction will be limited by the slower of these two reactions.

There is a wealth of information in the literature on the kinetics of electroless copper deposition on various substrates, many of them on experimentally determining the plating rate as a function of various solution components and conditions.[3-5] There has not been a great deal of work done on developing mathematical models for the electroless deposition processes. Paunovic[6] developed a computer model for studying the effect of pH on the deposition rate. Donahue[7] developed a mathematical study of electroless copper deposition by assuming diffusion to be the major mode of transfer of ions to the electrode surface. He also took into account equations for the microconvection resulting from the bubble formation and evolution at the substrate surface. Recently, Kim and Sohn[8] developed a mathematical model for the electroless plating of nickel on a rotating disk electrode under steady state. They used the concepts of mixed potential theory and applied the Butler-Volmer kinetics for determining the plating rate as a function of the various concentrations in solution at steady state. However, most of the experimental parameters such as the concentrations at the surface, pH, etc., vary at the electrode surface as a function of time. Since the equilibrium potential is a thermodynamic quantity that is dependent on the concentrations of the respective ions near the electrode surface, it also varies as a function of time thereby changing the rates of electroless plating significantly.

This paper presents the results obtained from the development of a time-dependent mathematical model for the electroless plating of copper based on fundamental principles. The experimental conditions used for the development of this mathematical model are described elsewhere.[9] The governing equations take into account mass transport by migration and diffusion, and mixed potential theory dictates the reaction rate. A copper-tartrate-formaldehyde bath is considered for the deposition process. Our previous study[9] showed the results obtained from the solution equilibrium studies on such a plating bath. It showed that at pH regions 11.0 and above, copper is completely complexed by tartrate and exists as $Cu(OH)_2L_2^{-4}$ ion, where L is the tartrate ligand. Hence, the reactions that were modeled in this study are

$$Cu(OH)_2L_2^{-4} + 2e^- \rightarrow Cu + 2\,OH^- + 2L^{-2} \quad [1]$$

$$2HCHO + 4\,OH^- \rightarrow 2HCOO^- + H_2 + 2H_2O + 2e^- \quad [2]$$

At very high pH values, formaldehyde has been found to exist as methylene glycolate ion.[3,10] However, for the purpose of this study, formaldehyde was assumed to not dissociate into the glycolate compound. Subsequent modeling efforts will include this equilibrium, and the effect this has on the plating rate.

Model Development

Figure 1 shows the schematic diagram of the electroless deposition process considered in this study. For the experimental conditions[9] and the reactions mentioned above, one could deduce the important dependent variables that need to be tracked in the system. These consist of eight ionic species [$Cu(OH)_2L_2^{-4}$, HCHO, $HCOO^-$, H^+, OH^-, SO_4^{-2}, Na^+, L^{-2}], the solution potential (Φ), and the electrode potential (V). The underlying assumptions in the model are (*i*) dilute solution theory is valid; (*ii*) transport of the material is one-dimensional and exists only in the direction normal to the electrode surface; (*iii*) the flux of all species is due to diffusion and migration only; (*iv*) the system is isothermal; (*v*) the bath volume is very large compared to the area of deposition, hence the bulk concentration

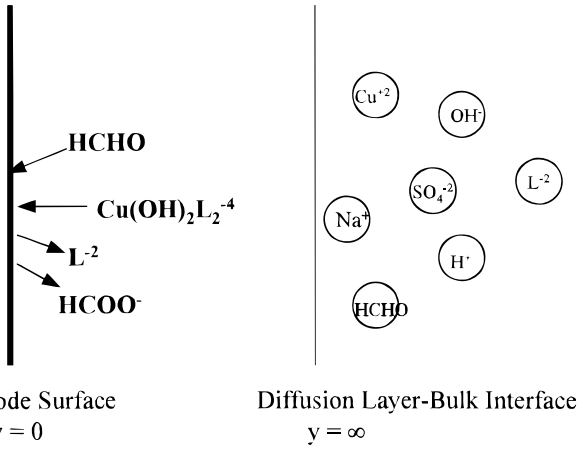

Figure 1. A schematic representation of the electroless plating modeling region on planar electrodes.

* Electrochemical Society Student Member.
** Electrochemical Society Active Member.

S0013-4651(98)02-031-X CCC: $7.00

does not change during deposition; and (*iv*) natural convection effects are negligible.

Equations.—In the diffusion layer, the concentration of each ionic species is governed by the following material balance equation

$$\frac{\partial C_i}{\partial t} = -\nabla \cdot N_i + R_i \quad [3]$$

where R_i is the rate of homogenous production of species i from all reactions. The flux of each species i is given by

$$N_i = -\frac{z_i D_i F C_i}{RT}\frac{\partial \Phi}{\partial y} - D_i \frac{\partial C_i}{\partial y} \quad [4]$$

This equation contains the contributions from migration and diffusion only. In solution, water equilibrium exists at all times and hence the equation

$$C_{H^+} C_{OH^+} - K_w = 0 \quad [5]$$

should be satisfied. The potential in the solution varied in accordance to the electroneutrality condition given by

$$\Sigma z_i C_i = 0 \quad [6]$$

The list of the governing equations for all the ten variables considered in this problem are given in Table I.

Boundary conditions and sign conventions.—At the diffusion layer-bulk interface, $y = \infty$, the concentrations of each of the eight species corresponds to its bulk values

$$C_i = C_i^b \quad [7]$$

The bulk equilibrium conditions are governed by the equations described in a previous study.[9] These eight equations, along with the electroneutrality constraint, give rise to the nine independent equations for the nine variables of interest in the bulk.

At the electrode surface, $y = 0$, the flux for each of the eight ionic species can be written as

$$N_i = -\frac{s_{ij} i_j}{n_j F} \quad [8]$$

In the above equation, i_j is the current density of either the reduction or the oxidation reaction. The cathodic current is assumed to have a negative sign, and the anodic current is assumed to have a positive sign. s_{ij} is the stoichiometric coefficient of species i in the electrochemical reaction j which is expressed for the reduction reaction (Eq. 1) as

$$\sum_i s_{ij} M_i^{z_i} \rightarrow n_j e^- \quad [9]$$

In the case of the formaldehyde oxidation reaction (Eq. 2), the stoichiometric coefficient is calculated by writing the reaction in a different form, as

$$n_j e^- \rightarrow \sum_i s_{ij} M_i^{z_i} \quad [10]$$

The stoichiometric coefficients are taken after writing these two reactions differently because of the need for consistency in the direction of the flux. A species that is consumed at the electrode should have a flux going into the electrode surface, irrespective of whether it is due to the oxidation or the reduction reaction. The stoichiometric coefficients for all the different species involved in the reactions are given in Table II.

The overall copper reduction reaction (Eq. 1) and the formaldehyde oxidation reaction (Eq. 2) may each consist of two or more elementary steps, the precise kinetic form of which is not known with certainty. However, one can couple the currents due to each of these elementary steps (as outlined by Newman[12]) and obtain expressions for the overall reaction rate in terms of the concentrations of the electroactive species. The partial current densities of the cathodic

Table I. Model equations for electroless copper deposition.

$y = \infty$ Diffusion layer-electrolyte interface	$0 < y < \infty$ Diffusion layer	$y = 0$ Electrode surface
$C_{Cu(OH)_2L_2^{-4}} = C^b_{Cu(OH)_2L_2^{-4}}$	$\frac{\partial C_{Cu(OH)_2L_2^{-4}}}{\partial t} + \nabla \cdot N_{Cu(OH)_2L_2^{-4}} = 0$	$N_{Cu(OH)_2L_2^{-4}} + \frac{s_{Cu(OH)_2L_2^{-4},1} i_1}{nF} = 0$
$C_{HCHO} = C^b_{HCHO}$	$\frac{\partial C_{HCHO}}{\partial t} + \nabla \cdot N_{HCHO} = 0$	$N_{HCHO} + \frac{s_{HCHO,2} i_2}{nF} = 0$
$C_{HCOO^-} = 0$	$\frac{\partial C_{HCOO^-}}{\partial t} + \nabla \cdot N_{HCOO^-} = 0$	$N_{HCHO} + \frac{s_{HCHO,2} i_2}{nF} = 0$
$C_{H^+} = C^b_{H^+}$	$-\frac{\partial C_{H^+}}{\partial t} - \nabla \cdot N_{H^+} + \frac{\partial C_{OH^-}}{\partial t} + \nabla \cdot N_{OH^-} = 0$	$N_{HCOO^-} + \frac{s_{HCOO^-,2} i_2}{nF} = 0$
$C_{OH^-} = C^b_{OH^-}$	$K_w - C_{H^+} C_{OH^-} = 0$	$N_{H^+} = 0$
$C_{SO_4^{-2}} = C^b_{SO_4^{-2}}$	$\frac{\partial C_{SO_4^{-2}}}{\partial t} + \nabla \cdot N_{SO_4^{-2}} = 0$	$N_{OH^-} + \frac{s_{OH^-,1} i_1}{nF} + \frac{s_{OH^-,2} i_2}{nF} = 0$
$C_{Na^+} = C^b_{Na^+}$	$\frac{\partial C_{Na^+}}{\partial t} + \nabla \cdot N_{Na^+} = 0$	$N_{Na^+} = 0$
$C_{L^{-2}} = C^b_{L^{-2}}$	$\frac{\partial C_{L^{-2}}}{\partial t} + \nabla \cdot N_{L^{-2}} = 0$	$N_{L^{-2}} + \frac{s_{L^{-2},1} i_1}{nF} = 0$
$\Sigma z_i C_i = 0$	$\Sigma z_i C_i = 0$	$\Sigma z_i C_i = 0$
$V = 0$	$V = 0$	$i_2 - i_1 = 0$

S0013-4651(98)02-031-X CCC: $7.00

Table II. Physical data and model parameters used in the simulations

Species	z_i	$D_i \times 10^5$ (cm^2/s)	$s_{i,1}$	$s_{i,2}$	$C_{i,bulk}$ (mol/cm^3)
$Cu(OH)_2L_2^{-4}$	−4	0.7[a]	−1	0	0.06×10^{-3}
HCHO	0	1.2[a]	0	−2	0.22×10^{-3}
$HCOO^-$	−1	1.454[b]	0	2	0.0
H^+	1	9.311[b]	0	0	0.63×10^{-15}
OH^-	−1	5.273[b]	2	−4	0.16×10^{-4}
SO_4^{-2}	−2	1.065[b]	0	0	0.06×10^{-3}
Na^+	1	1.334[b]	0	0	1.13×10^{-3}
L^{-2}	−2	0.794[b]	2	0	0.39×10^{-3}

[a] Assumed value.
[b] From Ref. 11.

and anodic reactions can be assumed to obey Butler-Volmer kinetics. If the reduction reaction goes through a number of steps, all of which are in series, and the intermediate species formed do not diffuse away from the electrode, the partial current density for copper reduction can be written as

$$i_1 = i_{o1,ref}\left\{\prod_i \left(\frac{C_{i,o}}{C_{i,ref}}\right)^{P_{i1}} \exp\left(\frac{\alpha_{a1}F}{RT}[V - \Phi_o - U_1^\theta]\right) - \prod_i \left(\frac{C_{i,o}}{C_{i,ref}}\right)^{q_{i1}} \exp\left(\frac{-\alpha_{c1}F}{RT}[V - \Phi_o - U_1^\theta]\right)\right\} \quad [11]$$

where $p_{i1} = s_{i1}$ when $s_{i1} > 0$ and $q_{i1} = s_{i1}$ when $s_{i1} < 0$. The terms in parentheses in the above equation signify the driving force for a one-electron transfer reaction to the $Cu(OH)_2L_2^{-4}$ complex forming an intermediate. Using the above-mentioned conditions of zero intermediate loss and series reactions, the overall current density for the cathodic reaction can be determined by multiplying a factor of two (number of electrons involved in the reaction) to the elementary Butler-Volmer expression in Eq. 11.[12] It is also worth noting here that the concentration profiles of the various components depend only on the overall reaction rate and hence the exact kinetics of these reactions are not necessary for this purpose.

A similar treatment of the overall formaldehyde oxidation reaction results in the current density for the formaldehyde oxidation reaction to be given by

$$i_2 = i_{o2,ref}\left\{\prod_i \left(\frac{C_{i,o}}{C_{i,ref}}\right)^{P_{i2}} \exp\left(\frac{\alpha_{a2}F}{RT}[V - \Phi_o - U_2^\theta]\right) - \prod_i \left(\frac{C_{i,o}}{C_{i,ref}}\right)^{q_{i2}} \exp\left(\frac{-\alpha_{c2}F}{RT}[V - \Phi_o - U_2^\theta]\right)\right\} \quad [12]$$

where $p_{i2} = s_{i2}$ when $s_{i1} < 0$ and $q_{i2} = s_{i2}$ when $s_{i1} > 0$.

In Eq. 11 and 12 the driving force for the electrochemical reaction is provided by the potential difference term $[V - \Phi_o - U_1^\theta]$. V is the electrode potential, Φ_0 is the solution potential adjacent to the electrode surface, and U_1^θ is the open-circuit potential for the reaction i. The open-circuit potential is calculated for these two reactions by a Nernst equation as

$$U_1^\theta = U_1^o + \frac{RT}{nF} \ln\frac{[Cu(OH)_2L_2^{-4}]}{[OH^-]^2[L^{-2}]^2} \quad [13]$$

$$U_2^\theta = U_2^o + \frac{RT}{nF} \ln\frac{[HCOO^-]^2}{[OH^-]^4[HCHO]^2} \quad [14]$$

where U_1^o and U_2^o are the standard electrode potentials for the reduction and oxidation reactions, respectively.

Since, during electroless plating, there is no net current flowing through any external system, the cathodic and anodic currents should be equal and opposite to each other and hence the following equation has to be satisfied at all times

$$i_1 + i_2 = 0 \quad [15]$$

Solution procedure.—The set of ten coupled nonlinear equations given in Table I along with the equations for the current density, 11 and 12, and the current constraint equation, 15, are solved by a finite difference procedure using Newman's BAND routine.[12] The governing equations were written using a three-point finite difference procedure using central differences. Three point backward and forward differences were used at $y = \infty$ and $y = 0$, respectively. The boundary condition signifying $y = \infty$ was placed at a fixed length along the y direction, which corresponds to a fixed diffusion layer thickness. The minimum thickness, at which there is an insignificant jump in the concentration profile between the bulk-diffusion layer interface and the adjacent node points in the diffusion layer, was assumed to be the thickness of the diffusion layer. This thickness was typically about 0.2 cm for all the conditions modeled in this study.

Model parameters.—The transport and kinetic parameters required for carrying out these calculations are detailed in Table II. The bulk concentrations of each variable under a given set of conditions were obtained using the procedure detailed in a previous publication. The standard electrode potential for the copper reduction reaction (U_1^o) was determined as follows.

The standard potentials tabulated by Shacham-Diamand et al.[13] for various copper complexes were taken and plotted against their respective pK_a values. This graph provided a straight line plot, which indicated that the degree of difficulty of reducing a metal from its complexed form is directly dependent on the strength of this complex formed. This plot was subsequently extrapolated for the pK_a value of $Cu(OH)_2L_2^{-4}$ and assumed as the standard potential for copper deposition from this complex. The electrode potentials assumed for the copper reduction and formaldehyde oxidation reactions are −0.266 and 1.5 V, respectively.

Results and Discussion

Figure 2 shows the predicted electrode potential during electroless plating for various combinations of copper complex and formaldehyde in the bath. One can see that there is a significant change in the potential in the positive direction during the initial stages of the deposition. The electrode potential, V, is the mixed potential that is realized as a result of the constraint in the current (Eq. 15). This mixed potential is also dependent on the open-circuit potentials for the reduction and oxidation reactions that are governed by the Nernst equations 13 and 14. As one can see from Eq. 13, the electrode poten-

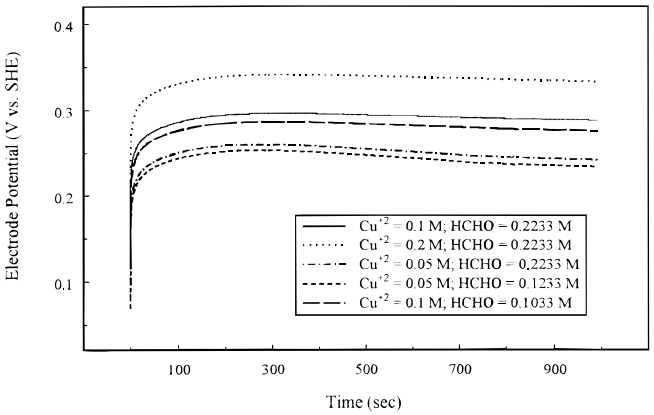

Figure 2. Predicted electrode potential values during electroless plating for various concentrations of copper and formaldehyde in the bath.

S0013-4651(98)02-031-X CCC: $7.00

tial is a function of the hydroxide ion concentration squared. One can also see from the electrochemical reactions that two hydroxide ions are consumed for each copper complex reduction. Hence, during the initial times of electroless plating, the hydroxide ion concentration would decrease significantly, thereby causing the open-circuit potential to move in the positive direction for both the anodic and cathodic reactions. Since we have assumed that the cathodic and anodic reaction transfer coefficients do not vary with concentration, a movement in the open-circuit potentials for these two reactions in the anodic direction would cause the resulting mixed potential to move in the positive direction. This movement in the mixed potential also causes the partial current densities to decrease considerably during the initial plating periods. Similar behavior of the overall potential at the electrode surface shifting rapidly during the initial stages of electroless plating has been observed experimentally, and the duration up to which this occurs has been termed as the induction period.[14] The existence of this induction period has also been attributed to the difference in the nature and properties of the substrate on which the deposition occurs as time progresses.[14]

It can also be seen from Fig. 2 that the mixed potential goes through a maximum and subsequently stabilizes at a value significantly positive of the potential at which the electroless plating started. The maximum in deposition potential occurs due to the competition between the variations in the open-circuit potentials. As we have noted before, the hydroxide ion concentration takes predominance in the early stages due to its initial concentration being diminished. However, at longer periods of time, the mixed potential for the cathodic reaction tends to shift in the cathodic direction because of the decrease in the copper complex concentration and a corresponding increase in the free tartrate ligand concentration. This causes the mixed potential to go through a maximum and subsequently shift in the cathodic direction. This stabilization in the mixed potential also causes stabilization in the current density for the most part, even though there is a slight further decrease in the current mainly due to the depletion of the reactants as a function of time. Figure 2 also shows the electrode potential responses obtained for various combinations of copper and formaldehyde concentrations. An increasing copper concentration causes a net shift in the mixed potential in the anodic direction. This is dictated in part by the Nernst equation, where the concentration of the complex increases and a corresponding decrease is observed in the concentration of hydroxide and that of free tartrate. Such a shift in the positive direction has also been experimentally observed by Bindra et. al.[16] for an ethylenediaminetetraacetic acid (EDTA) based bath. The magnitude of a shift is much less when the concentration of formaldehyde is increased keeping all other variables constant. An increase in formaldehyde contributes to an increase in current through the Butler-Volmer equation (Eq. 12), which causes additional depletion of hydroxide ion concentration, thereby contributing to a shift in the potential in the positive direction. However, the magnitude is less because the increasing formaldehyde concentration, by itself, tends to move the potential toward the cathodic direction as dictated by Eq. 14.

Figure 3 shows the predicted current density plot for the electroless copper plating from a bath containing 0.1 M $CuSO_4$, 0.2233 M HCHO at a pH of 12.25. The partial current density plot shows a very significant decrease in current density in the initial time periods closely following the potential plot shown in Fig. 2. At very short times, the driving force for the reaction, the difference between the open-circuit potential and the mixed potential for the cathodic and anodic reactions, is significantly high. Thus, the greater driving force causes a large current. Due to the movement of the open-circuit potentials in the positive direction and the concentration depletion at the surface, the polarization decreases with time causing the current to decrease rapidly. At subsequent times, the electrode potential stabilizes, which again causes the current and the corresponding surface concentrations to decrease.

Figure 4a shows a plot of the concentrations of various species at the surface for very short plating times. The concentrations of all the components that get consumed at the surface decrease very sharply

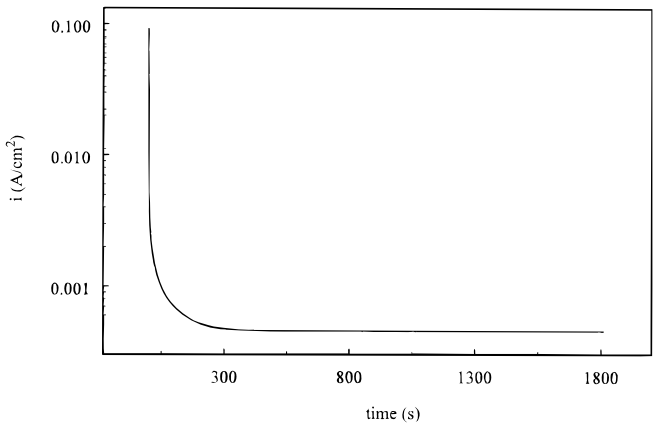

Figure 3. Electroless copper deposition current density as a function of time for a bath containing 0.1 M $CuSO_4$, 0.2233 M HCHO at a pH of 12.25.

during the initial periods and then increase due to the arrival of new ions from the bulk by diffusion and migration. The initial decrease in the concentrations of $Cu(OH)_2L_2^{-4}$ and HCHO is caused by the fast initial reaction rate. This depletion is offset by the diffusion and migration components of these species to a small extent, which causes the surface concentrations to recover. Similarly, the concentration of free tartrate increases rapidly, and subsequently decreases due to diffusion toward the bulk. Figure 4b shows similar plots for the sur-

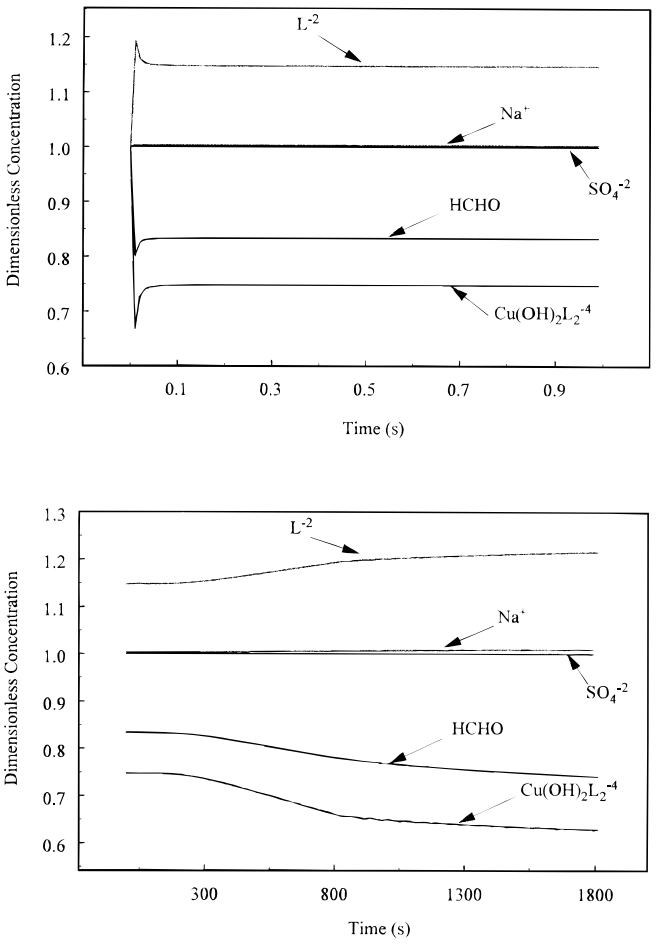

Figure 4. (a, top) Concentrations of the copper complex, formaldehyde, sulfate, sodium, and the free tartrate ligand (L^{-2}) at the electrode surface for very short times. (b, bottom) Concentrations of the species mentioned in Fig. 4a for longer times.

S0013-4651(98)02-031-X CCC: $7.00

face concentrations at larger times for these five species. The sulfate concentration does not change throughout the bath at all times due to its not being consumed at the electrode surface. The slight increase in the sodium concentration arises because of the need to maintain electroneutrality condition throughout the diffusion layer.

The dimensionless concentrations of $Cu(OH)_2L_2^{-4}$, HCHO, and L^{-2} can be divided into three regions: (*i*) the initial region from 10 to 200 s where the surface concentrations remain relatively constant; (*ii*) the intermediate time zone region between 200 and 800 s where the concentration decreases significantly; and (*iii*) the longer time regions where the concentration levels off.

The three regions can be further understood with the help of a plot of the concentration profiles from the bulk to the electrode surface for the copper complex presented in Fig. 5. One can see that there is very significant concentration depletion in the initial stages of deposition since the current density is very high. Subsequently a combination of the replenishment caused by mass transfer from the bulk and a rapid decrease in the current density causes the surface concentration to remain constant up to 200 s, thereby giving rise to the first region in Fig. 4b. Once the mass-transfer profile stabilizes at around 200 s, at subsequent times, the surface concentration starts to decrease because of the inability of the complex to reach the electrode surface. This phenomenon gives rise to the intermediate concentration depletion region in Fig. 4b. At significantly larger times, the plating current density decreases further and almost reaches a steady-state value as shown in Fig. 3. This also causes the concentration depletion to reduce thereby causing the third constant concentration region in Fig. 4b.

Figure 6 shows similar concentration profiles for the formaldehyde from the bulk to the surface. One can see that the formaldehyde concentration profiles also show a similar behavior as the copper complex, thereby giving rise to three regions in the surface concentration-time curve. The model was run for an electroless deposition period of 5 h, and the surface concentrations of $Cu(OH)_2L_2^{-4}$ and HCHO were still found to be 35 and 75% of their bulk values, respectively. Figure 7 gives a plot of the concentration profiles of the hydroxide ions as a function of time. The concentration of OH^- decreases rapidly, and the profile falls into a straight line even before 500 s of plating. One can see that the hydroxide ion tends to limit the electroless plating process, and the plating rate is predominantly dependent on the hydroxide ion concentration at the surface. Figure 8 shows the surface concentration of the hydroxide ion at various times during the plating process. For a pH of 12.25, the concentration is four orders of magnitude lower than that at the bulk. This significant decrease in OH^- ion concentration is due to the fact that the initial concentration of OH^- is significantly small when compared to both the copper complex and formaldehyde. Moreover, according to the mechanism taken into account in our model, two OH^- ions are consumed during the reduction of one copper ion. These factors contribute to a significant decrease in the hydroxide concentration. The initial stages of electroless plating have high currents because of the higher surface concentrations and lower polarization. These high currents cause a rapid decrease in the active species concentrations at the surface as seen in Fig. 8. However, at longer times, the deposition rate slows down and reaches a somewhat steady value that is dependent

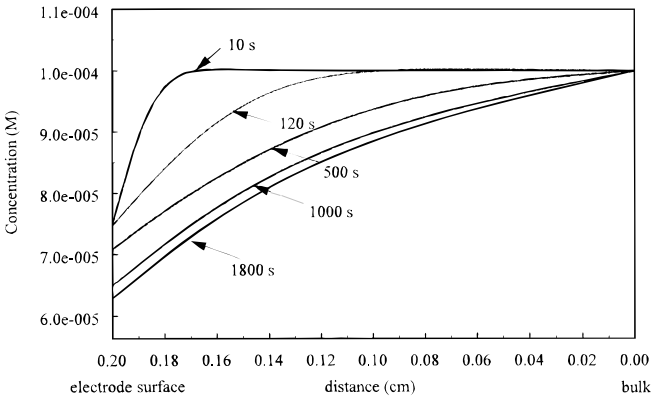

Figure 5. Concentration profiles between the bulk and the electrode surface for $Cu(OH)_2L_2^{-4}$ ion at different plating times.

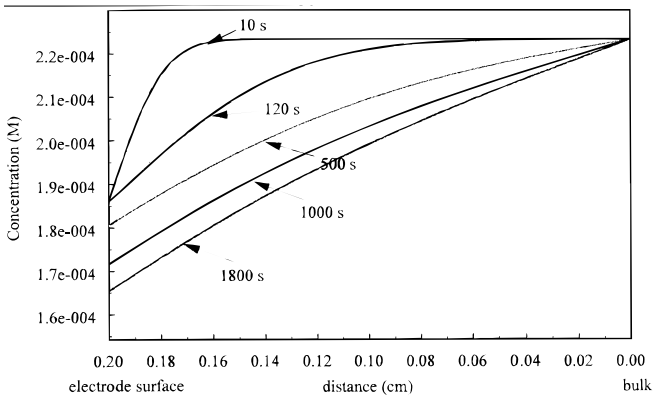

Figure 6. Concentration profiles between the bulk and the electrode surface for HCHO molecule at different plating times.

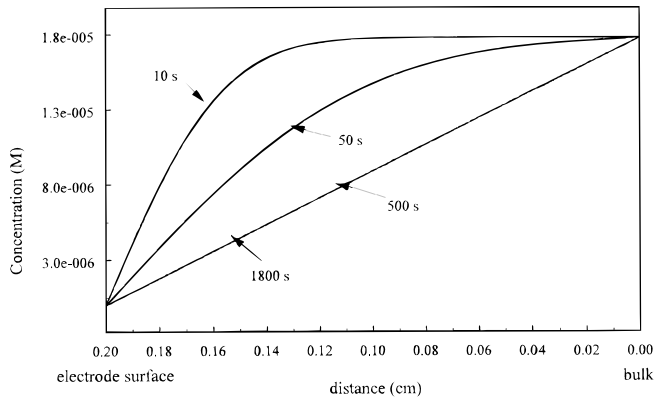

Figure 7. Concentration profiles between the bulk and the electrode surface for the hydroxide ion at different plating times.

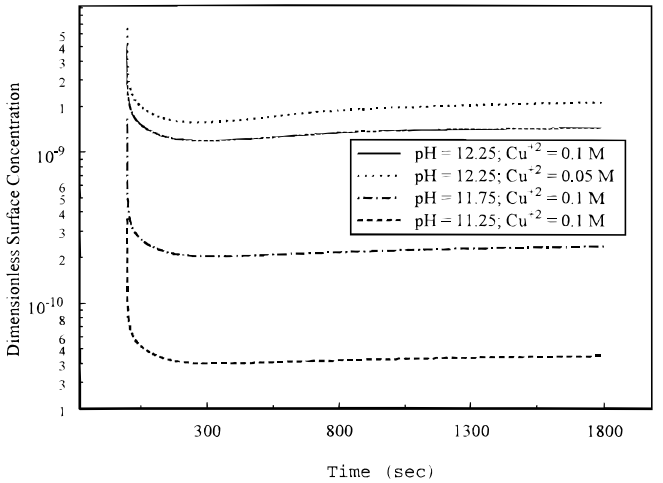

Figure 8. Concentration of OH^- at the surface as a function of time for three different bulk pH and two different bulk copper concentrations. The concentrations simulated for are (—) Cu^{+2} = 0.1 M, pH 12.25; (····) Cu^{+2} = 0.05 M, pH 12.25; (–·–·–) Cu^{+2} = 0.1 M, pH 11.75; (– – – –) Cu^{+2} = 0.1 M, pH 11.25.

S0013-4651(98)02-031-X CCC: $7.00

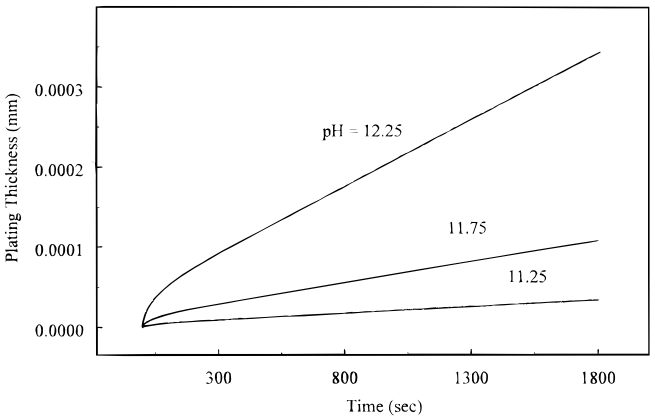

Figure 9. Electroless copper deposit thickness as a function of time for various bulk pH values.

chiefly on the hydroxide concentration at the surface. A decrease in the copper concentration changes the surface pH very slightly. This slight decrease in surface OH^- is due to a very slight decrease in the current with a decrease in copper concentration. According to the mechanism assumed, and the results obtained in Fig. 7 and 8, one can see that the plating rate will be influenced by pH more than any other parameter in the deposition process.

The copper deposit thickness as predicted by the model is plotted for various solution pH values in Fig. 9. In all the three pH ranges the model was run for, the partial current density was very high initially, and subsequently decreased significantly as witnessed by the change in slope of the plating thickness. Subsequently the current stabilizes, and we obtain a linear relationship of the plating thickness with time. Experimental studies carried out in the literature[17,18] have shown that there is a maximum that exists for the plating rate as a function of pH. This has been attributed to the dissociation of methylene glycol, which is formed under conditions of high pH. The model developed here does not take into account the formation or the subsequent dissociation of methylene glycol. An inclusion of the methylene glycol formation and the dissociation reaction equilibrium has to be done in order to predict the observance of a maximum in the plating rate.

Conclusions

A mathematical model for the electroless copper deposition on planar substrates from a copper-tartrate bath is presented. The model predicts the surface concentrations, electrode potential, and the plating rate as a function of different electroactive species concentrations in the bath. The predictions obtained for the electroless copper deposition from tartrate baths show that OH^- ion concentration is mass-transfer limited and hence dictates the plating rate.

Acknowledgment

This work was supported by the United States Department of Energy under contract DE-AL04-94AL8500. Sandia is a multiprogram laboratory operated by Sandia Corporation, a Lockheed Martin Company, for the United States Department of Energy.

The University of South Carolina assisted in meeting the publication costs of this article.

List of Symbols

C_i	concentration of species i, mol/cm^3
C_i^b	bulk concentration of species i, mol/cm^3
$C_{i,o}$	surface concentration of species i, mol/cm^3
$C_{i,ref}$	reference concentration of species i, mol/cm^3
D_i	diffusion coefficient of species i, cm^2/s
F	Faraday's constant, 96,487 C/quiv
i_j	current density due to reaction j, A/cm^2
$i_{oj,ref}$	exchange current density at reference concentrations for reaction j, A/cm^2
K_w	ionic product for water equilibrium, (mol/cm^3)^2
M_i^{zi}	symbol for species i with charge z_i
n_j	number of electrons transferred in reaction j
N_i	flux of a species i, mol/cm^2 s
p_{ij}	anodic reaction order of species i in reaction j
q_{ij}	cathodic reaction order of species i in reaction j
R	universal gas constant, 8.314 J kg^{-1} K^{-1}
R_i	net homogenous production of species i from all reactions, mol/cm^2 s
s_{ij}	stoichiometric coefficient of ionic species i in reaction j
t	time, s
T	temperature, K
U_i^o	standard electrode potential for reaction i, V
U_i^θ	open-circuit potential for reaction i, V
V	electrode potential, V
y	directional coordinate, cm
z_i	charge number of species i

Greek

α_{aj}	anodic transfer coefficient for reaction j
α_{cj}	cathodic transfer coefficient for reaction j
Φ	solution potential, V
Φ_0	solution potential at interface, V

References

1. M. Paunovic, *Plating*, **55**, 161 (1968).
2. F. M. Donahue, *J. Electrochem. Soc.*, **119**, 72 (1972).
3. F. M. Donahue, *Oberflache-Surf.*, **12**, 301 (1972).
4. S. M. El-Raghy and A. A. Abo-Salama, *J. Electrochem. Soc.*, **126**, 171 (1972).
5. F. M. Donahue, K. L. M. Wong, and R. Bhalla, *J. Electrochem. Soc.*, **127**, 2340 (1980).
6. M. Paunovic, *J. Electrochem. Soc.*, **132**, 173 (1978).
7. F. M. Donahue, *J. Electrochem. Soc.*, **127**, 51 (1980).
8. Y.-S. Kim and H.-J. Sohn, *J. Electrochem. Soc.*, **143**, 505 (1996).
9. M. Ramasubramanian, B. N. Popov, R. E. White, and K. S. Chen, *J. Appl. Electrochem.*, In press.
10. P. Bindra, J. M. Roldan, and G. V. Arbach, *IBM J. Res. Develop.*, **28**, 679 (1984).
11. *CRC Handbook of Thermophysical and Thermochemical Data*, D. R. Lide and H. V. Kehiaian, Editors, CRC Press, Inc., Boca Raton, FL (1994).
12. J. S. Newman, *Electrochemical Systems*, 2nd ed., Prentice Hall, Englewood Cliffs, NJ (1991).
13. Y. Shacham-Diamand, V. Dubin, and M. Angyal, *Thin Solid Films*, **262**, 93 (1995).
14. M. Paunovic, *J. Electrochem. Soc.*, **124**, 349 (1977).
15. M. Paunovic, in *Electrodeposition Technology, Theory and Practice*, L. T. Romankiw and D. R. Turner, Editors, PV 87-17, p. 349, The Electrochemical Society Proceedings Series, Pennington, NJ (1987).
16. P. Bindra, D. Light, and D. Rath, *IBM J. Res. Develop.*, **28**, 668 (1984).
17. L. N. Schoenberg, *J. Electrochem. Soc.*, **118**, 1571 (1971).
18. J. Duffy, L. Pearson, and M. Paunovic, *J. Electrochem. Soc.*, **130**, 876 (1983).